REDUCED BEAM SECTION WELDED STEEL MOMENT FRAMES

Scott L JONES[1], Gary T FRY[2] And Michael D ENGELHARDT[3]

SUMMARY

This paper presents results from SAC Task 7.06a, "Analysis and Testing of Reduced Beam Section Connections". Specifically, an elastic-plastic fibre model of the reduced beam section (RBS) region is presented. This model is used to determine the contribution to elastic-plastic story drift attributable solely to elastic-plastic RBS region deformation assuming all other elements as rigid: i.e. column, panelzone, and non-RBS portions of the beams. The proposed fibre model compares favourably with results from three-dimensional, elastic-plastic finite element analyses, and measurements from full-scale tests of cruciform-shaped moment frame subassemblies.

INTRODUCTION

During the 1994 Northridge, CA Earthquake, the beam flange-column flange weldments in steel moment resisting frames (SMRF) failed at much lower than anticipated load and drift levels. These failures have led structural engineers to improve upon the connection detailing used prior to the earthquake. Among these improvements are the use of a better weld material and welding process, the use of haunches at the beam-column interface (primarily intended for retrofit of damaged frames), the use of cover plates on the beam flanges at the beam-column interface, and the use of a reduced beam section (RBS) at a prescribed distance from the column face. The RBS appears to be the most economical of the new design methods and is already being used by structural engineers for welded SMRF structures in seismic zones.

The reduced beam section (RBS) protects a welded SMRF connection detail by forcing the plastic hinge in a beam to form away from the column face. Traditionally, welded SMRF connection design requires using a strong column-weak beam combination, which means that any instability in the frame would result from plastic hinging in the beams rather than the columns. With maximum moments occurring at the beam-column interface in moment frames under lateral loading, the plastic hinges will form at the column face, placing high strain demand on the weldment. The RBS reduces the moment capacity of the beam at a prescribed distance from the column face (between a and a+b/2 from the column face in Figure 1) and forces the large strains to occur in a more desirable location.

In order to verify the performance of the RBS, researchers have performed a series of experiments on full-scale welded SMRF connection details with a RBS. Chen et al (1996), Iwankiw and Carter (1996), and Zekioglu et al. (1997a, 1997b) investigated the performance of tapered cut RBS details in single-sided beam-column subassemblages (i.e. one beam attached to a column). Engelhardt et al (1996, 1997), Popov et al (1998), Tremblay et al (1997), Plumier (1990, 1997), and Uang (1998, 1999) performed tests on radius cut RBS details (Figure 1) in single-sided beam-column subassemblage tests after repeated fracture in taper cut RBS specimens. Engelhardt and Venti (1999) and Fry et al (1999) performed tests on radius cut RBS details in double-sided beam-column subassemblages (Figure 2) to account for higher demands on the panel zone in interior frame joints. All but one of the reported tests that have used a radius cut RBS detail and the new weld detail have performed as expected, with a plastic hinge forming in the RBS to protect the weldment.

[1] *Graduate Research Assistant, Department of Civil Engineering, Texas A&M University, College Station, TX 77843-3136 USA*
[2] *Assistant Professor, Department of Civil Engineering, Texas A&M University, College Station, TX 77843-3136 USA*
[3] *Associate Professor, Department of Civil Engineering, University of Texas at Austin, Austin, TX 78712 USA*

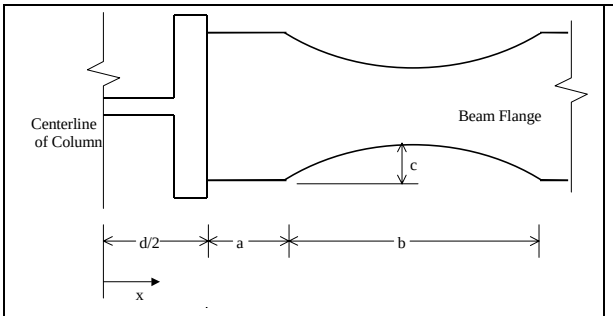

Figure 1. Radius-cut reduced beam section (RBS) detail.

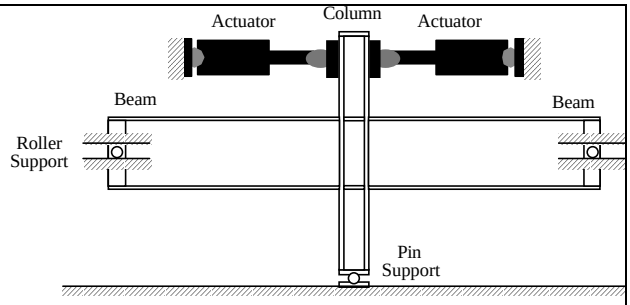

Figure 2. Double-sided moment frame subassemblage test set-up

REDUCED BEAM SECTION FIBRE MODEL

An elastic-plastic fiber model is presented herein to analyze the column tip load vs. RBS contribution to total story drift curve. Isolation of RBS material behavior requires that the rest of the material in the frame is treated as rigid forcing all of the deformation into the RBS (Figure 3). The model combines the concepts of static equilibrium of structures, Euler-Bernoulli Beam Theory (i.e. plane sections remain plane), and a uniaxial stress-strain relationship for steel to describe the story drift of the frame in Figure 2. Minor modifications to some of the equations below will yield a similar model for single-sided beam-column subassemblages. The method described below assumes that the specimen is geometrically perfect (no buckling) and that the weld material contains no imperfections (i.e. assuming *no* possibility of fracture). These assumptions imply that the model is only accurate in predicting a frame's displacement response to an applied load and vice versa. The engineer who uses this model must identify the limit states of the frame independent of this story drift analysis.

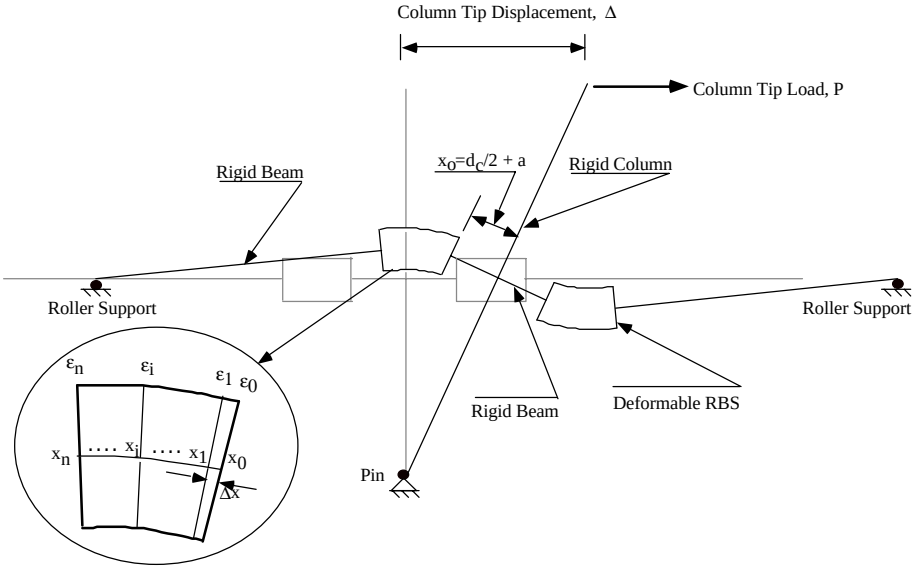

Figure 3. Rigid beam-column model with deformable RBS. The inset illustrates the fiber model parameters

Moment values at sections within the RBS can be calculated using simple static equilibrium. Summation of moments about the pin support yields the reactions at the beam-ends as follows:

$$R = \frac{Ph}{L} \tag{1}$$

where R is the vertical reaction in the roller supports, P is the laterally applied load at the column tip, h is the column height, and L is the distance between the two roller supports. Internal beam moment is then defined by:

$$M_1(x) = R\left(\frac{L}{2} - x\right) = \frac{Ph}{L}\left(\frac{L}{2} - x\right) \tag{2}$$

where $M_1(x)$ is the moment at a distance x from the centerline of the column.

The internal beam deformation must be described and a constitutive law must be used in order to determine the moment from the stress distribution. The strain distribution is assumed to be linear based on elementary beam theory as follows:

$$\varepsilon(x,y) = \phi(x)y \tag{3}$$

where $\phi(x)$ represents the beam curvature and ε is the strain at x from the centerline of the column and y from the centerline of the beam. The constitutive law used in this model follows:

$$\sigma(\varepsilon) = \begin{Bmatrix} E\varepsilon & \varepsilon \le \varepsilon_y \\ c_1\varepsilon^3 + c_2\varepsilon^2 + c_3\varepsilon + c_4 & \varepsilon > \varepsilon_y \end{Bmatrix} \tag{4a,b}$$

where σ is stress, E is Young's Modulus, and $\{c_1,\ldots,c_4\}$ are constants used to describe the inelastic material behavior. Constants used in this study are derived based upon data from standard tension tests of structural steel. The inelastic stress-strain relationship in equation 4b assumes the occurrence of kinematic hardening under cyclic loading, hence the exclusion of the yield plateau. Equilibrium of moments requires:

$$M_2(x) = 2\int_A y\sigma\left(\varepsilon(x,y)\right)dA \tag{5}$$

where $M_2(x)$ is the moment at a distance x from the centerline of the column and c is the distance from the center of the beam section to the top of the upper beam flange (or bottom of the lower beam flange). When a W-shape is discretized in y, equation 5 becomes:

$$M_2(x) = 2\left[\sum_{i=1}^{n}\frac{y_i + y_{i-1}}{2}\frac{\sigma_i + \sigma_{i-1}}{2}t_w\left(y_i - y_{i-1}\right) + \sum_{j=1}^{m}\frac{y_j + y_{j-1}}{2}\frac{\sigma_j + \sigma_{j-1}}{2}b_f\left(y_j - y_{j-1}\right)\right] \tag{6}$$

with the first term in brackets representing the contribution of half of the beam web (thickness t_w and height $d_b/2-t_f$) and the second term representing the contribution of the beam flange (width b_f and height t_f). The beam flange width varies along the length of the RBS and is described by:

$$b_f = b_{f0} + \frac{-b^2 + 4c^2 + \sqrt{\left(b^2 - 4c^2\right) - 16c^2\left(2a + d_c - 2x\right)\left(2a + 2b + d_c - 2x\right)}}{8c} \tag{7}$$

where b_f is the beam flange width at distance x from the column centerline, b_{f0} is the beam flange width of the beam outside of the RBS, d_c is the column depth, and a, b, and c are the shape parameters of the RBS as shown in Figure 2.

Next, the above equations must satisfy moment equilibrium for every value of x within the RBS. $\phi(x)$ must be determined at a discrete number of x values along the RBS via an iterative moment matching process. Assume a value for $\phi(x)$, determine the corresponding internal moment, and compare it to the known external moment. Next, adjust $\phi(x)$ according to the equation:

$$\phi = \phi_0 + \phi_0\frac{M_1 - M_2}{M_1} \tag{8}$$

until the internal moment, $M_2(x)$, equals the external moment, $M_1(x)$.

Finally, the story drift is determined by discretizing the RBS in x and calculating the strains that correspond with the moments in equations 2 and 6. The contribution of each discrete segment of the RBS, assuming constant curvature, to the total story drift is described by:

$$\Delta_k = \frac{2\varepsilon_k \ell_k h}{d_b}\left(\frac{2\left(\frac{L}{2}-\frac{d_c}{2}-x-\ell_k\right)+\ell_k}{L}\right) \tag{9}$$

where Δ_k is the story drift contributed by a section of the RBS l_k long. The RBS can be broken into small enough parts such that an assumption of constant curvature gives an accurate approximation of story drift. Combining the contributions from each of the RBS segments gives the total story drift attributable to the RBS:

$$\Delta = \sum_{k=1}^{l} \frac{(\varepsilon_k + \varepsilon_{k-1})(dx)h}{d_b}\frac{L - d_c - 2x_k - dx}{L} \tag{10}$$

where Δ is the total story drift contributed by the RBS and dx is the length of each segment in the discretized RBS. Column tip load vs. RBS contribution to story drift curves can be developed for any welded SMRF frame with a radius cut RBS by repeating the above procedures for a range of P values

FINITE ELEMENT ANALYSES

Two finite element models of full-scale beam-column welded SMRF sub-assemblages used in experiments were developed to predict measurements of response and to validate the RBS fibre model. The finite element models were generated and post-processed in MSC/PATRAN (1996) and solved using ABAQUS (1998). The models consisted of 24,334 nodes and 23,972 S4R four-node reduced-integration shell elements. The node at the center of the column web at the bottom of the column was restrained in the x and y directions and nodes at the center of the beam web at the free end of each beam were restrained in the y direction only. The nodes on the right column flange at the top of the column were displaced in the x direction. Figure 4 depicts an isoparametric view of the deformed finite element mesh with the undeformed geometry and corresponding boundary conditions in the background. All finite element models contained nonlinear material properties and were thus run in several time steps up to peak displacement.

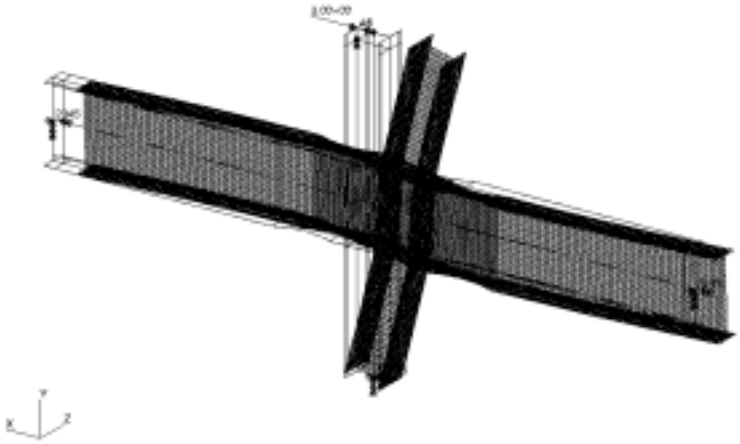

Figure 4- Finite element model of beam-column subassemblage

The three frames used in finite element models consist of W14x398 0r W14x283 columns and W36x150 beams with two slightly different radius cuts. The first specimen consists of a 12’ W14x398 column and two 12’ W36x150 beams fully welded at the beam-column flange interface. The RBS on both beams has the following dimensions: a=9”, b=27”, and c=3”. The second specimen consists of a W14x398 column with ¾” doubler-plates on both sides of the column web in the panel zone and W36x150 beams with the same RBS and beam-column attachment as above. Weld geometry was neglected in the finite element models and the weld material properties were assumed to be identical to the steel base metal properties. Although the effects of such treatment of the weld properties are critical when considering local material stress and strain demands, they are insignificant with regard to modelling global performance of the system.

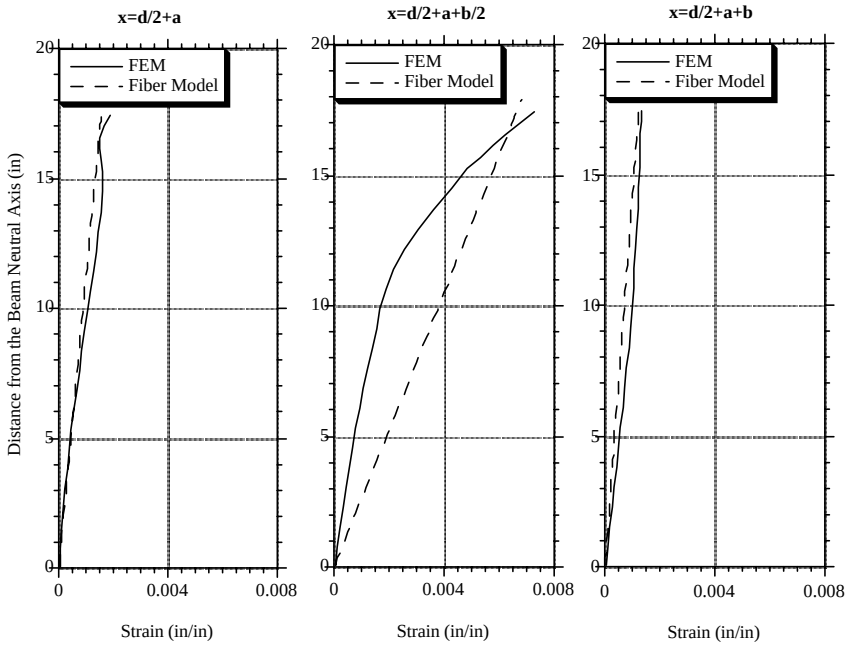

Figure 5. RBS elastic-plastic strain distributions predicted by the fiber and finite element models.

The RBS contribution to the story drift according to the finite element model was calculated in the same way as for the RBS fiber model outlined above. PATRAN outputs the strain at each node in the model, allowing the user to apply equation 10 to the finite element model with dx equal to the element length. For specimen 1, axial strain distributions according to the finite element model are compared to the assumed linear axial strain distributions from the fiber model at several points along the RBS in Figure 5. The discrepancies between strain distributions in the two models result from differences in assumptions between shell finite element modeling and Euler-Bernoulli Beam Theory, specifically because Euler-Bernoulli Beam Theory neglects warping resulting from shear deformation of the beam (Popov, 1990). Despite the differences in the strain distributions, the column tip load vs. RBS contribution to total story drift curves are nearly identical as evidenced in Figure 6.

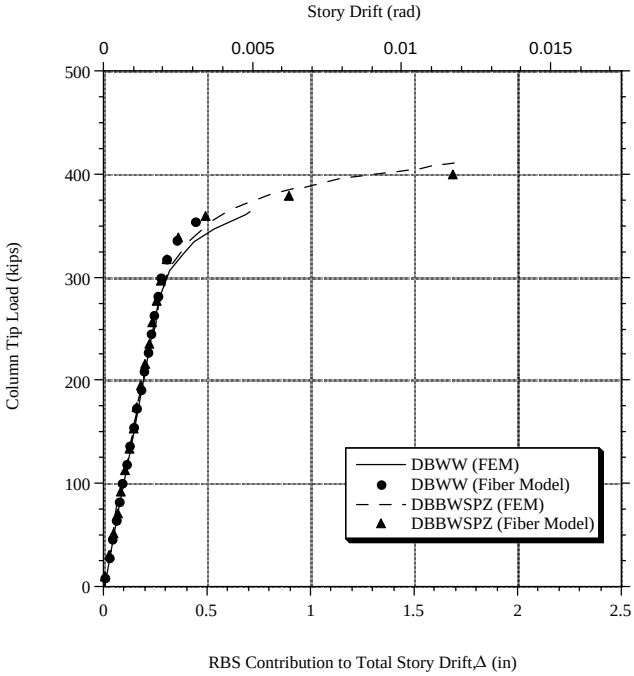

Figure 6. Comparison of fiber model with finite element model results for two cruciform subassemblages.

FULL-SCALE TESTS

Experiments were performed on full-scale double-sided specimens (Figure 2) in the structural engineering laboratory at Texas A&M University. Two such tests, denoted DBWW and DBBWSPZ , were similar to the finite element models described above. The beam flanges were field welded to the column flanges with complete joint penetration single bevel groove welds made with the self-shielded flux cored arc welding process using an E70T-6 electrode. The bottom flange backing bars were removed and a small reinforcing fillet was placed at the root of the groove weld. The top flange backing bars were left in place and sealed with a fillet weld at its base. For specimen DBWW, the beam webs were field welded to the column flange with complete joint penetration single bevel groove welds made with the self-shielded flux cored arc welding process using an

E71T-8 electrode. For specimen DBBWSPZ, the beam webs were bolted to shear tabs that had been shop welded to the column flanges.

The experiments were designed to emulate the deformation of an unbraced SMRF subjected to lateral loading. To this end, the column base was pin-connected to the lab floor and the beam ends were restrained from moving vertically by bearing guides supported by vertical reaction frames (see Figure 2). Two 220-kip actuators supported by horizontal reaction frames applied the lateral column tip load. Figure 7 is a photograph of the experimental set-up with a specimen in place.

Each specimen was loaded cyclically, with the load amplitude increasing incrementally at pre-determined cycles, until either failure of one of the components occurred or the limits of the testing equipment was reached, according to specific loading protocol. In both specimens, saturation load corresponded to local buckling of the beam webs and flanges in the RBS region. For the purposes of comparison, only the experimental results up to peak load are considered.

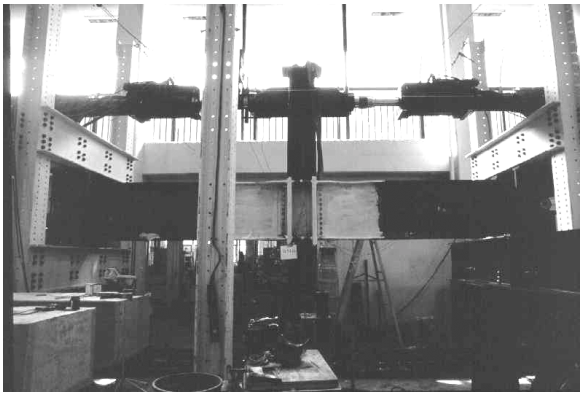

Figure 7. Photograph of experimental set-up using double-sided moment frame subassemblage.

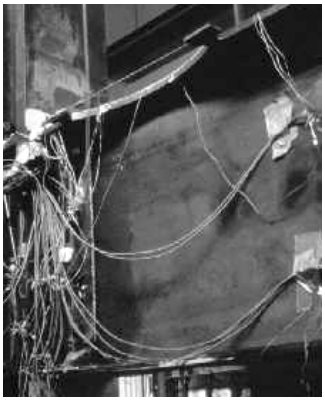

Figure 8. LVDTs spanning the RBS to measure the RBS contribution to column tip displacement.

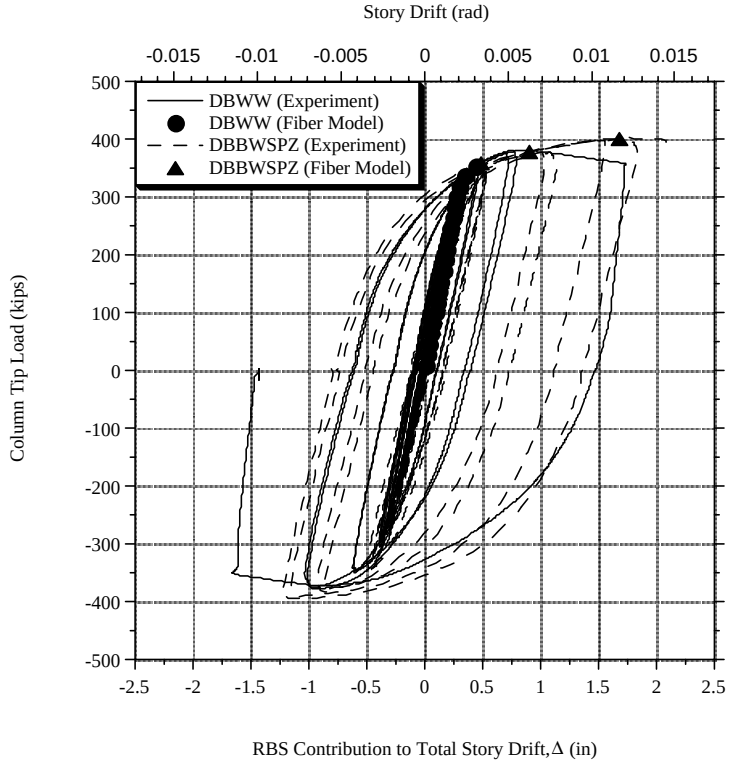

Figure 9. Comparison of results from the fiber model to experimental.

Both specimens were instrumented to measure the contribution of the individual components (i.e. beam, column, and panel zone) to column tip displacement according to SAC protocol. LVDTs, attached to the beam flanges with 100 lb. magnets, spanned the length of the RBS (Figure 8) to measure the axial deformation of the beam flanges. The RBS contribution to the column tip displacement can be approximated by:

$$\Delta = \frac{2\delta h}{d_b}\left(\frac{L - d_c - 2a - b}{L}\right) \tag{11}$$

which assumes that the curvature is constant across the deformed RBS. In actuality, the curvature will vary across the RBS but equation 11 still gives a reasonable approximation of the RBS contribution to story drift. Figure 9 shows an excellent agreement between the results from the fiber model and experimental results.

IMPLICATIONS FOR DESIGN

The fiber model developed in this study might be used to account for the RBS contribution to the deformation of a frame under lateral loading. Methods currently exist for predicting the response of a moment frame to static lateral loading using an elastic analysis. A designer could account for the change in flexibility of a frame with an RBS by making a few simple calculations. 1) Calculate the frame response using existing design methods. 2) Calculate the RBS contribution to the total story drift using the fiber model. 3) Use the fiber model to calculate the contribution of an equivalent section of beam without any reduction of section. 4) Subtract the result from step 2 from the results from step one and add the remainder to the result from step 1. The final result of this analysis is a reasonable prediction of the frame stiffness by adding a few steps to an existing method.

The curves developed using this fiber model might also be used, in addition to similar curves for the other beam and column components, to predict the total response of a frame to lateral loading. Analysis of the results from the finite element models presented above suggests that the inelastic material behavior is almost entirely isolated within each individual component of the frame. Since the plasticity does not seem to overlap from one component to another, similar models might be developed for the other components and summed to give the total story drift of a beam-column subassemblage under static lateral load. One current design method for structures subjected to seismic loads involves applying static lateral loads to each story level. With the response of each subassemblage to loading known, these loads could be distributed to beam-column subassemblages in a story by assuming a relationship for the relative story drift of frames within a structure (i.e. no relative motion if the slab is assumed to be rigid). Current methods for resolving earthquake loads in a structure might therefore be adapted using the methodology in this study.

Similarly, the curves developed using the fiber model might be used, in addition to other component curves, to predict the response of a structure to dynamic loading. A dynamic analysis would require a cyclic hardening rule for steel.

CONCLUSIONS

The fiber model presented in this paper provides structural engineers with a reliable method for predicting the RBS contribution to the elastic-plastic response of welded steel SMRFs to static lateral loading. Although the model gives reasonable predictions for the material deformation in the RBS, the designer must bear in mind that he/she is responsible for determining the material limit states as this model does not predict local buckling or fracture in the RBS. The designer is also responsible for considering any of the other material limit states for the frame.

ACKNOWLEDGEMENTS

This work was coordinated under the auspices of the SAC Joint Venture and supported financially by the Federal Emergency Management Agency and units within the Texas A&M University System (the Texas Engineering Experiment Station, the Department of Civil Engineering, and the Center for Building Design and Construction). The authors wish to thank the following individuals for invaluable assistance: James Malley, Stephen Mahin, Charles Roeder, Robert Dodds, Stanley Rolfe, John Barsom, Subhash Goel, Bozidar Stojadinovic and . Loren Lutes.

REFERENCES

ABAQUS v5.8 (1998). Hibbitt, Karlsson, & Sorenson, Inc.

Chen, S.J., Yeh, C.H. and Chu, J.M. (1996). "Ductile Steel Beam-to-Column Connections for Seismic Resistance," *J. Struct. Engrg.*, ASCE, 122(11), 1292-1299.

Engelhardt, M.D., Winneberger, T., Zekany, A.J. and Potyraj, T.J. (1996). "The Dogbone Connection, Part II, *Modern Steel Construction*.

Engelhardt, M.D., Winneberger, T., Zekany, A.J. and Potyraj, T.J. (1997). "Experimental Investigation of Dogbone Moment Connections," *Proceedings; 1997 National Steel Construction Conference*, American Institute of Steel Construction, Chicago.

Engelhardt, M.D. and Venti, M. (1999). Unpublished preliminary test reports for SAC Phase 2 tests, University of Texas at Austin.

Fry, G., Jones, S. L., and Holliday, S. D. (1999). Unpublished preliminary test reports for SAC Phase 2 tests, Texas A & M University.

International Building Code 2000 Final Draft (1998). International Code Council, Inc.

Iwankiw, N.R., and Carter, C. (1996). "The Dogbone: A New Idea to Chew On," *Modern Steel Construction*.

MSC/PATRAN v7.6 (1996). MacNeal-Schwendler Corporation.

Plumier, A. (1990). "New Idea for Safe Structures in Seismic Zones," *IABSE Symposium - Mixed Structures Including New Materials*, Brussels.

Plumier, A. (1997). "The Dogbone: Back to the Future," *Engrg. J.*, American Institute of Steel Construction, Inc. 2nd Quarter.

Popov, E. P. (1990). *Engineering Mechanics of Solids*, Prentice-Hall, Inc., Englewood Cliffs, New Jersey, Chapters 6-7.

Popov, E.P., Yang, T.S. and Chang, S.P. (1998). "Design of Steel MRF Connections Before and After 1994 Northridge Earthquake," *Engrg. Struct.*, 20(12), 1030-1038, 1998.

Tremblay, R., Tchebotarev, N. and Filiatrault, A. (1997). "Seismic Performance of RBS Connections for Steel Moment Resisting Frames: Influence of Loading Rate and Floor Slab," *Proceedings, Stessa '97*, Kyoto, Japan.

Uang, C.M. (1998). Unpublished preliminary test reports for SAC Phase 2 RBS tests, University of California at San Diego.

Uang, C.M. (1999). Unpublished preliminary test reports for SAC Phase 2 RBS tests, University of California at San Diego.

Zekioglu, A., Mozaffarian, H., and Uang, C.M. (1997a). "Moment Frame Connection Development and Testing for the City of Hope National Medical Center," *Building to Last - Proceedings of Structures Congress XV*, ASCE, Portland.

Zekioglu, A., Mozaffarian, H., Chang, K.L., Uang, C.M. and Noel, S. (1997b). "Designing After Northridge," *Modern Steel Construction*.

NOTATION

The following symbols are used in this paper:

A = area;

a = distance from exterior column flange face to beginning of reduced beam section;

b = length of reduced beam section;

b_f = beam flange width;

b_{f0} = original beam flange width;

c = depth of radius cut of reduced beam section;

c_1, c_2, c_3, c_4 = constants defining stress-strain relationship at strains greater than yield strain;

d_b = beam depth;

d_c = column depth;

E = Young's modulus;

h = column height;

i, j, k = summation indices;

L = span between the free ends of the beams in a double-sided beam-column subassemblage;

l = increment of RBS for fiber model;

l, m, n = summation limits;

M_1 = beam moment as determined by structural equilibrium;

M_2 = beam moment as determined by beam internal equilibrium;

P = column tip lateral load;

R = beam end vertical reaction;

t_f = beam flange thickness;

t_w = beam web thickness;

Δ = story drift;

δ = RBS LVDT displacement reading;

ε = strain;

ε_y = yield strain;

ϕ = beam curvature;

ϕ_0 = initial beam curvature estimate;

σ = stress.